Check for updates

Lanthanum-based metal organic framework (La-MOF) use of 3,4-dihydroxycinnamic acid as drug delivery system linkers in human breast cancer therapy

Moosareza Safinejad[1], Amir Rigi[2], Malihe Zeraati[3], Zohreh Heidary[4], Shohreh Jahani[5],
Narendra Pal Singh Chauhan[6] and Ghasem Sargazi[5*]

Abstract

Metal organic frameworks (MOFs) have received a lot of attention in the research community due to their unique physical properties, which make them ideal materials for targeted drug delivery systems. In this paper, we describe the synthesis of a non-toxic La-based MOF with 3,4-dihydroxycinnamic acid (3,4-DHCA) as a linker. Scanning electron microscopy (SEM), transmission electron microscopy (TEM), energy dispersive spectroscopy (EDS), fourier transform infrared (FTIR) spectroscopy, thermogravimetric analysis (TGA), nitrogen adsorption–desorption measurements, and X-ray powder diffraction (XRD) have all been used to characterize it thoroughly. The La-based MOF showed good biocompatibility with the human breast cancer cell line MDA-MB-468. The ability of 3,4-DHCA to treat MDA-MB-468 cells was confirmed by 40.35% cell viability with La-based MOF. Based on the findings, La-based MOF can be recommended as a promising candidate for anticancer delivery.

Keywords: Synthesis, Metal organic framework, Linker, Characterization, Drug delivery, Anticancer

Introduction

A group of lattice solids characterized by crystallization and porosity are called metal–organic frameworks (MOF), and major research has been done on the shape, surface, and pore measurements [1, 2]. The MOF compounds are the result of the binding of metal cations by organic ligands and are used in various fields, including drug delivery [3], gas storage [4], luminescent [5] and anticancer [6]. Due to the adjustable construction and chemical properties that change and function, MOF has many advantages over other drug delivery systems [7–9]. However, the high porosity and large surface area of MOFs have resulted in high loading and adsorption capacity, so poor coordination interaction ensures the biodegradability of MOFs [10]. MOFs have a major impact on colloid stability, cell uptake, and drug release profiles, [11, 12]which is highly desirable for pharmaceutical applications due to its surface properties and size [13]. MOFs have anti-cancer properties, for example Cu-MOF [14], Al-MOF [15], Sr-MOF [16], Co-MOF [17], Zn-MOF [18] and Zr-MOF [19] mentioned. Several research articles have recently reported on MOF and MOF-derived nanocomposites as gas sensor [20–22]. Nguyen and coworkers developed porous zeolitic imidazolate frameworks for fluorescent chemosensors [23], and the same group developed Zr-MOF as a nano adsorbent to remove toxic organic dye for water remediation [24]. Dang and coworkers developed Hf-MOF and Fe(III)-MOF using a one-pot three-component reaction

*Correspondence: g.sargazi@gmail.com

[5] Noncommunicable Diseases Research Center, Bam University of Medical Sciences, Bam, Iran

Full list of author information is available at the end of the article

Safinejad *et al. BMC Chemistry*   (2022) 16:93

Page 2 of 9

with high porosity and surface area for catalytic applications [25, 26].

3,4-Dihydroxycinnamic acid contributes to plant defence mechanisms against predators, pests, and infections by inhibiting the growth of insects, fungi, and bacteria and promoting the protection of plant leaves against ultraviolet radiation B (UV-B) [27, 28]. CA and its derivatives have been studied in vitro and in vivo, and numerous physiological effects, such as antibacterial [29, 30], anti-hepatocarcinoma (HCC) [31], antioxidant [30, 32, 33], anti-inflammatory [30, 32, 33], anticancer [32, 33], and anti-hepatocellular carcinoma activity [34] have been demonstrated. HCC (hepatocellular carcinoma) is one of the leading causes of cancer death worldwide, hence anti-HCC activity is essential [35]. As a result, additional research on the chemical and pharmacological properties of CA is required to contribute to the future development of a novel medicine and, as a result, the extension of therapeutic possibilities [31]. Recently, Rao and coworkers have reviewed the development of MOFs for both in vivo and in vitro drug delivery application [36]. Chemodynamic therapy (CDT) and chemo photodynamic therapy (CPT), which inhibits tumors cell growth and division, are recognized as a potential pharmacological technique used to treat cancer [37, 38]. Tan and coworkers evaluated and discussed various MOFs for their CDT use [39]. Table 1 lists various MOFs and their preparation routes, crystallite size, BET surface area, and action on cell lines.

Lanthanum has recently been reported as an effective drug for the treatment of malignant tumors. For example, in human cervical carcinoma cells, lanthanum complex has shown significant cytotoxicity in the laboratory [45–47]. $LaCl_3$ also reduced the growth and triggered apoptosis in leukemia cell lines, HL-60 and NB4 [48]. Furthermore, lanthanum has been linked to the inhibition of human stomach cancer cells' proliferation [49]. All of these findings revealed that lanthanum, a rare earth element, has the ability to regulate tumor growth [50].

In this study, lanthanum-MOFs (La-MOFs) with linkers of 3,4-dihydroxycinnamic acid (3,4-DHCA) was prepared with a ultrasonic reverse micelle assisted. it was characterized using XRD, TEM, EDS and TGA. It was also tested for anticancer properties.

Experimental
Materials and apparatus

Sigma-Aldrich Corporation was chosen to purchase $C_{12}H_{25}NaSO_4$ (sodium dodecyl sulfate) and 8 mL of C_6H_{14}. Merck & Co., Inc. was selected to prepare $La(NO_3)_3 \cdot 6H_2O$ (lanthanum nitrate hexahydrate) and $C_9H_8O_4$ (3,4-dihydroxycinnamic acid).

Each material has been of analytical grade with the increased purity. The Iranian Biological Resource Center (IBRC; Tehran, Iran) provided a human breast cancer (MDA-MB-468) cell line. Trypsin/EDTA solution, 3-(4,5-dimetylthiazol-2-Yl)−2,5−diphenyltetrazolium bromide (MTT), Dulbecco's modified Eagle's medium (DMEM), fetal bovine serum (FBS), phosphate-buffered saline (PBS), and dimethyl sulfoxide (DMSO) were acquired from Gibco BRL and Sigma, respectively. They were developed in DMEM (Gibco, UK) supplemented with 10% FBS (Gibco) and 1% penicillin–streptomycin (Gibco) and incubated at 37 °C in a 5% CO_2 environment. During the synthesis of MOF, X-ray diffraction (XRD) was used to analyze and determine the crystalline structure and phases. To accomplish this goal, a powder X-ray diffractometer (Expert MPD, pananalytical, CuK = 0.154.6 nm) was employed in the $2\theta = 0–50$ degree range with a step width of 0.01 degree. The surface morphology was investigated using a scanning electron microscope (FESEM, FEI Nanosem 450). Adsorption/desorption measurements (BET, Belsorp mini II) at 77 K in N_2 environment were used to assess the porosities, surface area, and pore textural features of samples. Under an Argon environment, thermogravimetric analysis (TGA, TA Q600 USA) was performed from room temperature to 400 °C at a heating rate of 10 °C/min. The cell viability was determined using an ELISA reader (Bio-Tek, Elx 808, Germany) at k = 545 nm.

Table 1 MOFs and their anticancer activities on various cell lines

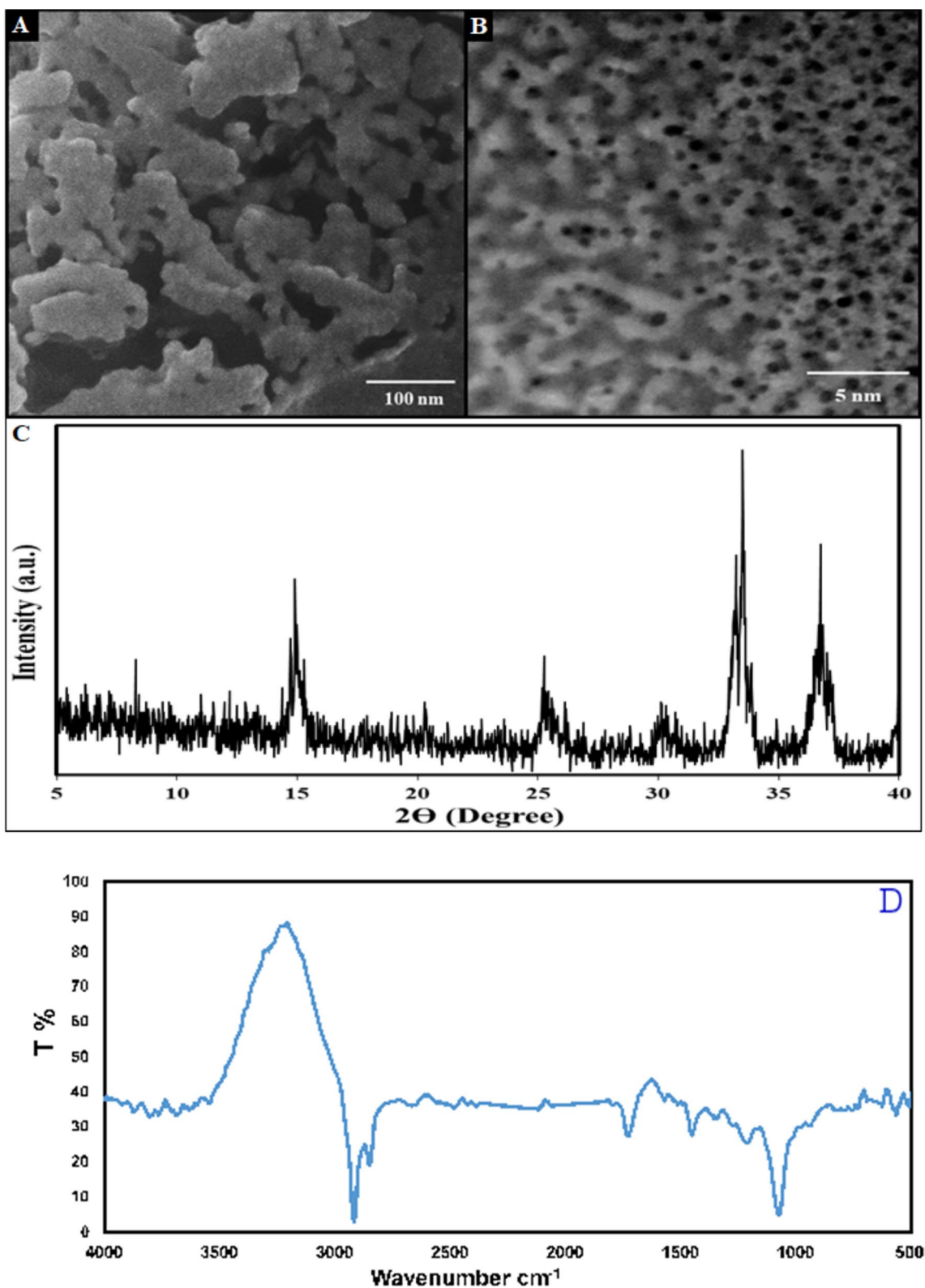| MOFs	Methods	Particle size; surface area	Cell line	Refs.
Cu-MOF	Ultrasonic assisted reverse micelle	less than 100 nm; 284.94 m²/g	MCF-7	[18]
Y-MOF	Microwave and ultrasonic irradiation	25 nm, 1267 m²/g	MCF-7	[40]
Doxorubicin@Zr-MOF)	One-pot conventional synthesis	−	MCF-7 and HepG-2	[41]
Zeolitic imidazolate crystal framework	One-pot conventional synthesis	250 nm; 495.199 m² g − 1	MCF-7	[42]
Nano Zr-MOF	One-pot conventional synthesis	less than 100 nm; 2296 m²/g	MCF-7/ADR cell and CD44	[43]
5-fluorouracil loaded Cu-MOF	One-pot conventional synthesis	281 nm, 628 m²/g	A549 and HeLa	[44]
Co-MOF	Solvo-thermal synthesis	less than 100 nm; 865 m²/g	HepG, CHO, HeLa, BEAS-2B, MDA-MB-231 and NCI-H460	[45]

Safinejad *et al. BMC Chemistry*   (2022) 16:93

Page 3 of 9

Fig. 1 **A** FE-SEM image and **B** TEM image. **C** XRD pattern **D** FT-IR spectrum of the La-based MOF

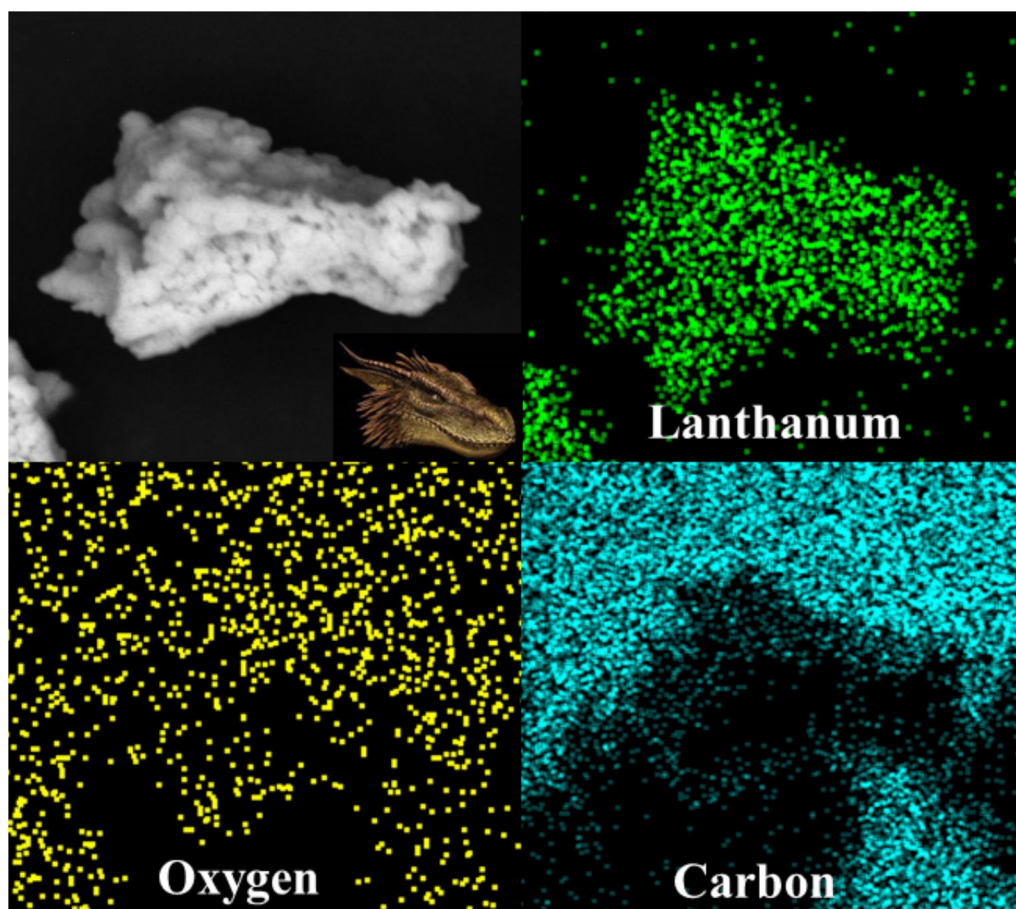Safinejad *et al. BMC Chemistry*   (2022) 16:93

Page 4 of 9

Fig. 2 EDX map images of La-based MOF. Inset: Digital photograph of a dragon's head

Preparation of aqueous extract of *satureja hortensis*

To make *S. hortensis* aqueous extract, combine 25 g of dry Satureja cut (harvested from Golboft in Kerman province of Iran, 2018) in clevenger-type apparatus with 250 mL of distilled water for 1.5 h, then cool and filter three times with centrifugal spinning machine at 3000 rpm. The extract was kept in refrigerator for future uses.

We confirmed that all the relevant permission to collect *S. hortensis* were obtained from the governing body. We are thankful to Prof. Gholamhossein Shahidi Bonjar who undertook the formal identification of the *S. hortensis* used in our study. The voucher ID for this plant was 18/D3713.
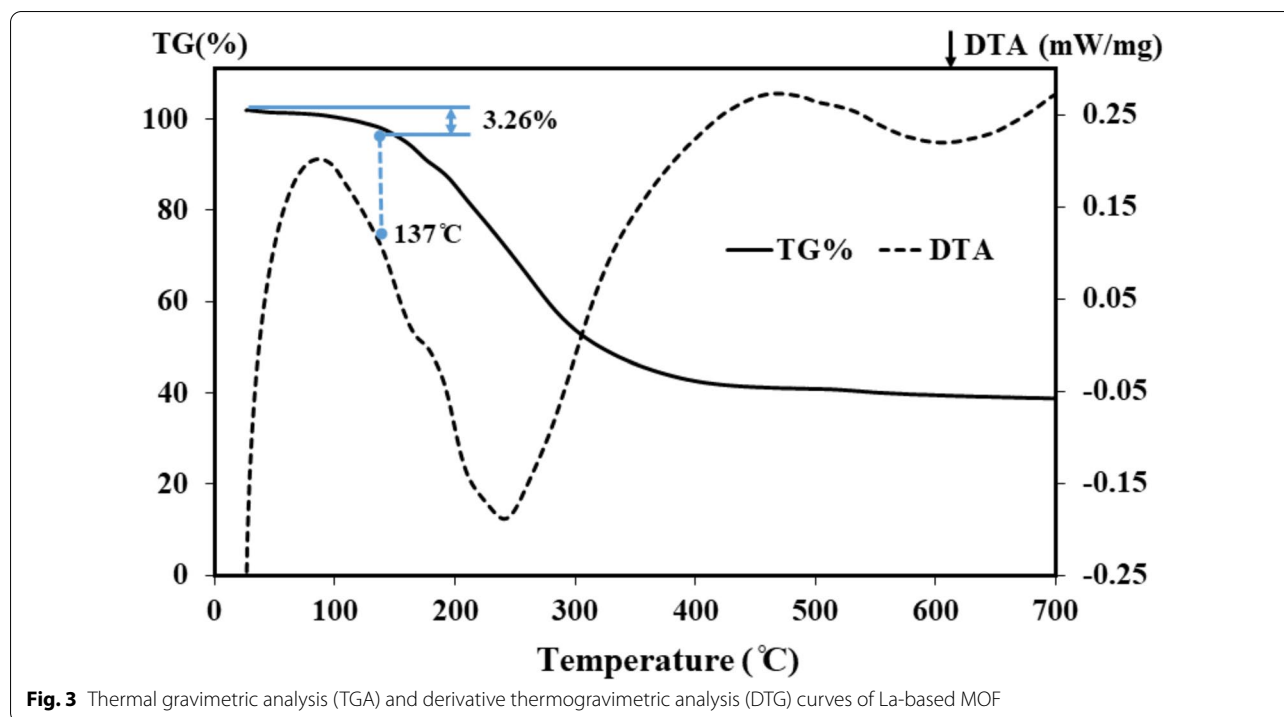
Synthesis of La-based MOF

During the preparation of the specimens using the ultra-sonic aided approach, $La(NO_3)_3.6H_2O$ (Control group: 19.0 g NaCl, 16.0 g KCl, 3.0 g $C_5H_8NO_4Na$ and 1.1 g $C_{12}H_{22}O_{11}$). and 3,4-DHCA were mixed with 1:1 mmol and dissolved in 21 mL of double distilled water. The resultant solution was mixed with 0.077 mmol sodium dodecyl sulphate and 8 mL hexane. The resulting mixture was then agitated for 1 h at 85 °C. The obtained solution was placed in the ultrasonic device and exposed to ultrasonic irradiation under optimal conditions, which included an ultrasonic time of 21 min, an ultrasonic temperature of 40 °C, and a power of 175 W. After 30 min, La-MOF crystals develop, which are centrifuged and washed with DMF. Using 75% of the ultrasonic power at 80 °C, a very high yield of 92.31% La-MOF was obtained.

Cytotoxicity

To begin treatment, 5×10^3 cells/well were seeded in 96-well flat-bottomed plates overnight; the cells were then subjected to different doses of the herbal extract (0–100.0 M) and La-based MOF (0–100.0 M) for 48 h. After removing the medium, 200 μL of MTT solution (5 mg/mL in PBS) was applied to each well and incubated for 4 h at 37 °C. Following the removal of the solution, 100 μL of DMSO was added to the plates, which were shaken for 15 min. Using an ELISA microplate reader, the absorbance of each sample was measured at 570 nm.

Safinejad *et al. BMC Chemistry*   (2022) 16:93

Page 5 of 9

Fig. 3 Thermal gravimetric analysis (TGA) and derivative thermogravimetric analysis (DTG) curves of La-based MOF

The results were expressed as a percentage of cell viability compared to untreated control cells.

Results

The surface morphology of the La-based MOF was studied by SEM micrograph (Fig. 1A and B). The crystallite size, phase structure and crystallinity of the La-based MOF were studied by XRD analysis. The XRD spectrum of La-based MOF is shown in Fig. 1C. The thermogravimetric analysis of the La-based MOF was carried out to determine the exact temperature needed for its decomposition. This could be further experimentally confirmed by the EDX elemental analysis of the sample shown in Fig. 2. Figure 3 illustrates the thermal analysis of La-based MOF as a final product. N_2 adsorption–desorption analysis was used to explore the textural features of La-based MOF.

Figure 5 shows how the MTT test was used to assess the anticancer activity of the La-based MOF and 3,4-DHCA in a human breast cancer cell line in vitro.

Discussion

Characterization of the La-based MOF

In the SEM image of La-based MOF can be seen uniform surface morphology (Fig. 1A). Besides, the TEM image of La-based MOF displayed that the surface of La-based MOF was uniform with many cavities in the internal zones. Therefore, this structure is capable to diffuse water into the beads and release the 3,4-DHCA (Fig. 1B).

The seven characteristic diffraction peaks of La-based MOF appeared at $2\theta = 14.95°$, $20.29°$, $25.27°$, $30.19°$, $33.28°$, $35.56°$ and $36.80°$ (Reference code: 96–450-4165) (Fig. 1C). No extra-diffraction peak in the XRD spectrum confirms the excellent purity and crystallinity of the La-based MOF. The crystallite size of the synthesized La-based MOF was estimated by Debye–Scherrer formula (Eq. 1).

$$D = \frac{0.9\lambda}{\beta cos\theta} \tag{1}$$

Here, λ stands for the wavelength of X-ray (1.54056 Å for Cu lamp), θ stands for half of the Bragg diffraction angle and β stands for half of the width of maximum intensity diffraction peak. The mean crystallite size of La-based MOF was 42 nm.

The FTIR spectrum of La-MOF is depicted in Fig. 1D. The La-MOF structure contains surface water, which causes the O–H broad stretching band to appear at 3387 cm^{-1}. C–H stretching is responsible for a sharp band at 2911 cm^{-1}. The bands shown at 1602 and 1377 cm^{-1} are attributed to the coordinated carboxylate's asymmetrical and symmetrical stretching modes, respectively. According to C–O stretching in La-MOF, a band that developed at 1139 cm^{-1}.
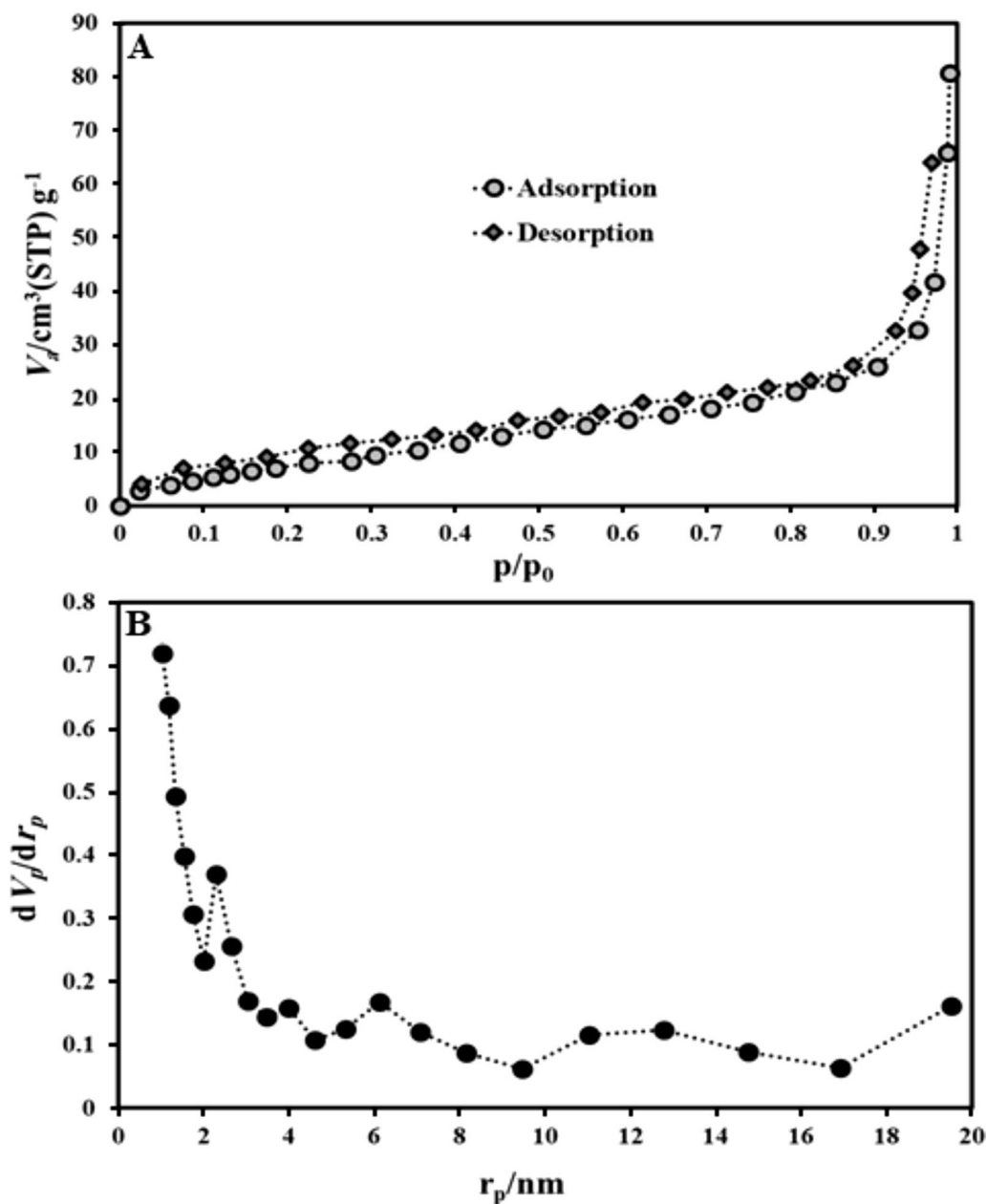
Safinejad *et al. BMC Chemistry*   (2022) 16:93

Page 6 of 9

Fig. 4 **A** N_2 adsorption–desorption isotherms La-based MOF; **B** BJH results obtained for La-based MOF

As seen in Fig. 2, the EDS mapping images for La-based MOF confirmed uniformly dispersion of each lanthanum, carbon and oxygen elements. If we consider the shape of the MOF as a dragon head, the distributions of the elements are as follows: the scattering of lanthanum is regularly on the dragon head and the carbon is evenly distributed on the background of the dragon head and the oxygen is evenly distributed throughout.

TGA-DTA thermograms for La-based MOF is shown in Fig. 3. La-MOF exhibit a two stage decomposition process. The first stage decomposition starts at 150–204 °C, which may be due to removal of bound water and carboxylate groups as CO_2 present in the La-MOFs. In the second stage, the main decomposition starts at 270 °C and end up at 450 °C, which corresponds to the loss of side chain attached to the aromatic nucleus. La-MOF exhibits reasonable thermal stability even at high temperatures, as confirmed by TGA and DTA data.

Figure 4a depicts type IV hysteresis loops in the prepared La-based MOF. This isotherm demonstrates the
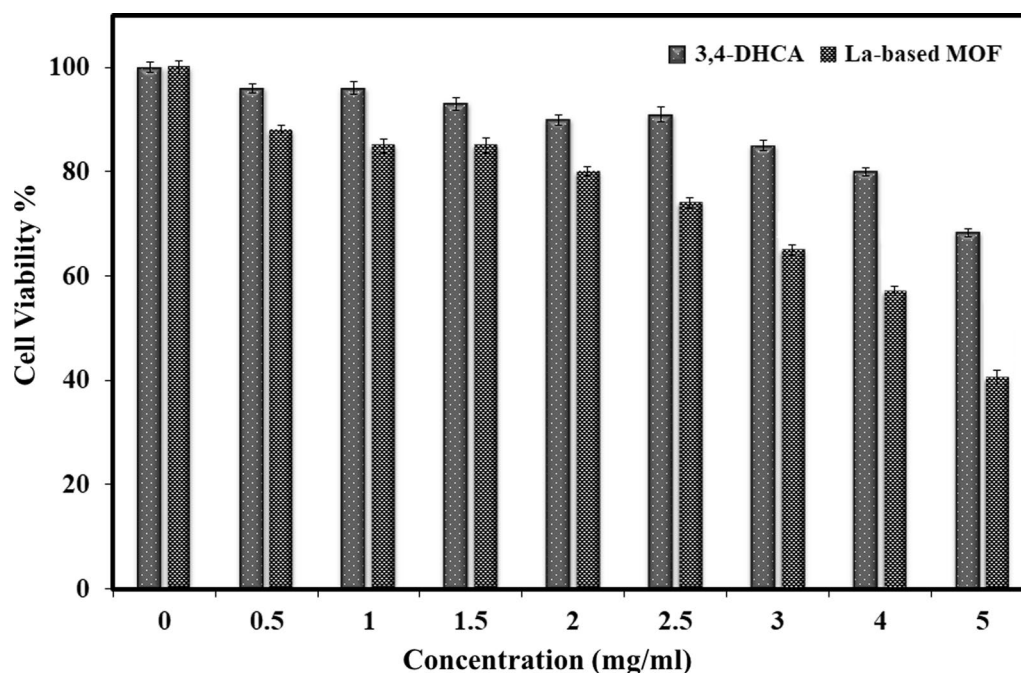
Safinejad *et al. BMC Chemistry*   (2022) 16:93

Page 7 of 9

Fig. 5 Plots of percentage of cytotoxicity vs. concentrations of the 3,4-DHCA (0–100.0 µM) and La-based MOF (0–100.0 µM) against human breast cancer cells after incubation for 48 h

mesoporous structure of the material and the parallel plate shaped pore. The obtained structural parameters such as BET surface area and pore volume of the La-based MOF were 521 $m^2.g^{-1}$ and 0.075 $cm^3.g^{-1}$, respectively. Figure 4B illustrates the pore size distribution of the La-based MOF samples on the basis of the Barrett–Joyner–Halenda (BJH) method. This figure also illustrates that the mean pore size distribution of the La-based MOF samples is 8.3 nm, which means the microporous size distributions of the products. It may be an indicative that the La-based MOF remained a wide pore opening and a high porosity, leading to the La-based MOF is one of the best carrier.

In vitro cytotoxicity studies
The values of cell viability found for the La-based MOF and 3,4-DHCA are 40.35% and 68.29%, respectively. Figure 5 shows that the La-based MOF antitumor behavior is greater compared to the 3,4-DHCA. La-based MOF passes through the cell membrane more easily than 3,4-DHCA. Thus, it facilitates the penetration of La-based MOF into cancer cells while improving its antitumor behavior. The anticancer behavior of La-based MOF may be described according to the concept of chelation. The polarity of metal ions may be significantly reduced by chelation because the positive charge is partly shared with the donor groups and

also due to the displacement of electrons in the chelate ring. The concentration of metal ions may be exacerbated by the lipophilic properties of chelates and the interaction between the cell wall and metal ions. The geometries and charge dispersion of the La-based MOF molecule are compatible with the cancer cell wall, which increases penetration through the cell wall. Such a unique structural arrangement can break down the cell's permeability barrier and disrupt the normal process of the cell.

Conclusion
Summery, in the first step, La-based MOF was prepared and characterized. The preparation of La-based MOF was approved by the SEM, TEM, EDX, TGA, BET and XRD analysis. In addition, in vitro anticancer activity results showed that La-based MOF can inhibit the growth of MDA-MB-468 cells line as a human breast cancer cell. The anticancer activity of the La-based MOF was more than in the 3,4-DHCA. Based upon the results of corresponding experiments, La-based MOF exhibited high 3,4-DHCA drug loading, cancer-targeted release and good biocompatibility, which can be used as a good candidate for anticancer drug delivery system.

Safinejad *et al. BMC Chemistry*　　(2022) 16:93

Page 8 of 9

Availability of data and materials

The datasets used and/or analyzed during the current study available from the corresponding author on request. We confirms all the relevant permission to collect sample were obtained from governing body.

Declarations

Ethics approval and consent to participate:

All methods were used in accordance with relevant guidelines and regulations. Also, we confirmed that all experimental protocols were approved by the Ethics Licensing Committee of the Bam University of Medical Sciences (no. 06 on 17/03/2021). MCF-7 cells were isolated from the pleural effusion of a 58-year-old woman with metastatic disease. In addition, informed consent was obtained from all study participants. We confirm that all the experimental research and field studies on wild plant ***satureja hortensis***, including the collection of plant material, were carried out in accordance with relevant institutional, national, and international guidelines and legislation.
Consent for publication.
Not applicable.

Competing interests

There is no competing interests.

Author details

[1]RF MEMS & Micro Bio-Nano Electronics (MBNE) Lab, Department of Electrical Engineering, Shahid Bahonar University of Kerman, Kerman, Iran. [2]Department of Nursing, Young Researchers and Elite Club, Zahedan Branch, Islamic Azad University, Zahedan, Iran. [3]Department of Materials Engineering, Shahid Bahonar University of Kerman, Kerman 761694111, Iran. [4]Vali-E-Asr Reproductive Health Research Center, Family Health Research Institute, Tehran University of Medical Sciences, Tehran, Iran. [5]Noncommunicable Diseases Research Center, Bam University of Medical Sciences, Bam, Iran. [6]Department of Chemistry, Bhupal Nobles' University, Udaipur-313002, Rajasthan, India.

References

1. Hu P, Morabito J, Tsung C. ACS Catal. 2014, 4, 4409.(d) Furukawa, H.; Cordova, KE; O'Keeffe, M.; Yaghi, OM. Science. 2013;341:1230444.
2. Gelfand BS, Taylor JM, Shimizu GK. Extracting structural trends from systematic variation of phosphonate/phosphonate monoester coordination polymers. CrystEngComm. 2017;19(27):3727–36.
3. Osterrieth JW, Fairen-Jimenez D. Metal-organic framework composites for theragnostics and drug delivery applications. Biotechnol J. 2021;16(2):2000005.
4. Chen S, Li Y, Mi L. Porous carbon derived from metal organic framework for gas storage and separation: the size effect. Inorg Chem Commun. 2020;118: 107999.
5. Brunckova H, et al. Preparation and characterization of isostructural lanthanide Eu/Gd/Tb metal-organic framework thin films for luminescent applications. Appl Surf Sci. 2021;542: 148731.
6. Ahmadijokani F, et al. Aluminum-based metal-organic frameworks for adsorptive removal of anti-cancer (methotrexate) drug from aqueous solutions. J Environ Manage. 2021;277: 111448.
7. Zhou T, Li J, Liu P. Ionically crosslinked alginate-based nanohydrogels for tumor-specific intracellular triggered release: effect of chemical modification. Colloids Surf, A. 2018;553:180–6.
8. Li X, et al. Preparation and characterization of a pH-responsive mesoporous silica nanoparticle dual-modified with biopolymers. Colloids Surf A. 2018;548:61–9.
9. Jiang Q, et al. Planar-structure perovskite solar cells with efficiency beyond 21%. Adv Mater. 2017;29(46):1703852.
10. He Z, et al. Hybrid nanomedicine fabricated from photosensitizer-terminated metal-organic framework nanoparticles for photodynamic therapy and hypoxia-activated cascade chemotherapy. Small. 2019;15(4):1804131.
11. Dang YT, et al. Microwave-assisted synthesis of nano Hf-and Zr-based metal-organic frameworks for enhancement of curcumin adsorption. Microporous Mesoporous Mater. 2020;298: 110064.
12. Nguyen LH, et al. Pore engineering of biomolecule-based metal–organic framework nanocarriers for improving loading and release of paclitaxel. New J Chem. 2022;46(14):6630–5.
13. Wang H, et al. One-pot synthesis of poly (ethylene glycol) modified zeolitic imidazolate framework-8 nanoparticles: size control, surface modification and drug encapsulation. Colloids Surf A. 2019;568:224–30.
14. Liu W, et al. A porous Cu (II)-based metal-organic framework carrier for pH-controlled anticancer drug delivery. Inorg Chem Commun. 2020;111: 107675.
15. Zeraati M, et al. Green synthesis and mechanism analysis of a new metal-organic framework constructed from Al (III) and 3, 4-dihydroxycinnamic acid extracted from satureja hortensis and its anticancerous activities. J Mol Str. 2021;1250: 131712.
16. Feng X-E, Zhu T-T. A porous Sr (II)-organic framework for 5-fluorouracil delivery and anti-cancer activity against human melanoma cells. Inorg Nano Metal Chem. 2020;50(12):1302–7.
17. Xi Y, et al. A New Co (II)-based metal-organic framework for size-selective cyanosilylation reaction and anti-cancer activity against lung cancer cell via inducing apoptosis. J Inorg Organomet Polym Mater. 2020;30(6):2204–12.
18. Akhavan-Sigari R, et al. Porous Cu-MOF nanostructures with anticancer properties prepared by a controllable ultrasound-assisted reverse micelle synthesis of Cu-MOF. BMC Chem. 2022;16(1):1–7.
19. Hassabo AA, et al. Immobilization of l-methioninase on a zirconium-based metal–organic framework as an anticancer agent. J Mater Chem B. 2019;7(20):3268–78.
20. Doan TLH, et al. Preparation of n-ZnO/p-Co3O4 heterojunctions from zeolitic imidazolate frameworks (ZIF-8/ZIF-67) for sensing low ethanol concentrations. Sens Actuators B Chem. 2021;348:130684.
21. Doan TLH, et al. Facile synthesis of metal-organic framework-derived ZnO/CuO nanocomposites for highly sensitive and selective H2S gas sensing. Sens Actuators B Chem. 2021;349:130741.
22. Lee J-H, et al. Functionalization of zirconium-based metal–organic frameworks for gas sensing applications. J Hazard Mater. 2021;403:124104.
23. Nguyen DT, et al. Zeolitic imidazolate frameworks as an efficient platform for potential curcumin-based on/off fluorescent chemosensor. Microporous Mesoporous Mater. 2021;327: 111445.
24. Nguyen LHT, et al. Microwave-assisted solvothermal synthesis of defective zirconium-organic framework as a recyclable nano-adsorbent with superior adsorption capacity for efficient removal of toxic organic dyes. Colloid Interface Sci Commun. 2022;46: 100511.
25. Dang M-HD, et al. Using sulfate-functionalized Hf-based metal–organic frameworks as a heterogeneous catalyst for solvent-free synthesis of pyrimido [1, 2-a] benzimidazoles via one-pot three-component reaction. J Ind Eng Chem. 2021;103:340–7.
26. Dang M, et al. Effect of Fe (III)-based MOFs on the catalytic efficiency of the tandem cyclooxidative reaction between 2-aminobenzamide and alcohols. New J Chem. 2020;44(34):14529–35.
27. Tošović J. Spectroscopic features of caffeic acid: theoretical study. Kragujevac J Sci. 2017;39:99–108.

Safinejad *et al. BMC Chemistry*   (2022) 16:93

Page 9 of 9

28. Gould KS, et al. Functional role of anthocyanins in the leaves of *Quintinia serrata* A. Cunn. J Exp Bot. 2000;51(347):1107–15.
29. Verma RP, Hansch C. An approach towards the quantitative structure–activity relationships of caffeic acid and its derivatives. ChemBioChem. 2004;5(9):1188–95.
30. Genaro-Mattos TC, et al. Antioxidant activity of caffeic acid against iron-induced free radical generation—a chemical approach. PLoS ONE. 2015;10(6): e0129963.
31. Zhang Z, et al. Metabolic and microbial signatures in rat hepatocellular carcinoma treated with caffeic acid and chlorogenic acid. Sci Rep. 2017;7(1):1–10.
32. Huang Q, Lin Y, Yan Y. Caffeic acid production enhancement by engineering a phenylalanine over-producing *Escherichia coli* strain. Biotechnol Bioeng. 2013;110(12):3188–96.
33. Lin Y, Yan Y. Biosynthesis of caffeic acid in *Escherichia coli* using its endogenous hydroxylase complex. Microb Cell Fact. 2012;11(1):1–9.
34. Gu W, et al. Caffeic acid attenuates the angiogenic function of hepatocellular carcinoma cells via reduction in JNK-1-mediated HIF-1α stabilization in hypoxia. RSC Adv. 2016;6(86):82774–82.
35. McGlynn KA, Petrick JL, London WT. Global epidemiology of hepatocellular carcinoma: an emphasis on demographic and regional variability. Clin Liver Dis. 2015;19(2):223–38.
36. Rao C, et al. Novel formulations of metal-organic frameworks for controlled drug delivery. Exp Opin Drug Del. 2022;19:1–20.
37. Ding Q, et al. A multimodal metal-organic framework based on unsaturated metal site for enhancing antitumor cytotoxicity through chemo-photodynamic therapy. J Colloid Interface Sci. 2022;621:180–94.
38. Pan Y, et al. A versatile and multifunctional metal–organic framework nanocomposite toward chemo-photodynamic therapy. J Solid State Chem. 2020;49(16):5291–301.
39. Tan X, et al. Recent advances in nano-architectonics of metal-organic frameworks for chemodynamic therapy. J Solid State Chem. 2022;314:123352.
40. Saleh RO, et al. Synthesis of bioactive yttrium-metal–organic framework as efficient nanocatalyst in synthesis of novel pyrazolopyranopyrimidine derivatives and evaluation of anticancer activity. Front Chem. 2022;10:743.
41. El-Bindary MA, El-Desouky MG, El-Bindary AA. Metal–organic frameworks encapsulated with an anticancer compound as drug delivery system: Synthesis, characterization, antioxidant, anticancer, antibacterial, and molecular docking investigation. Appl Organomet Chem. 2022;36(5):e6660.
42. El-Bindary AA, et al. Metal–organic frameworks as efficient materials for drug delivery: synthesis, characterization, antioxidant, anticancer, antibacterial and molecular docking investigation. Appl Organomet Chem. 2020;34(11):e5905.
43. Kim K, et al. MOF×biopolymer: collaborative combination of metal–organic framework and biopolymer for advanced anticancer therapy. ACS Appl Mater Interfaces. 2019;11(31):27512–20.
44. Liu W, et al. A porous Cu (II)-based metal-organic framework carrier for pH-controlled anticancer drug delivery. Inorg Chem Commun. 2020;111:107675.
45. Kapoor S. Lanthanum and its rapidly emerging role as an anti-carcinogenic agent. J Cell Biochem. 2009;106(2):193–193.
46. Durgo K, et al. Cytotoxic and genotoxic effects of the quercetin/lanthanum complex on human cervical carcinoma cells in vitro. Arh Hig Rada Toksikol. 2011;62(3):221–6.
47. Shen L, et al. Proteomic analysis of lanthanum citrate-induced apoptosis in human cervical carcinoma SiHa cells. Biometals. 2010;23(6):1179–89.
48. Dai Y, et al. Effects of rare earth compounds on growth and apoptosis of leukemic cell lines. In Vitro Cell Dev Biol Anim. 2002;38(7):373–5.
49. Shi P, Huang Z. Proteomic detection of changes in protein synthesis induced by lanthanum in BGC-823 human gastric cancer cells. Biometals. 2005;18(1):89–95.
50. Zhang J, et al. Recent progress in therapeutic and diagnostic applications of lanthanides. Mini Rev Med Chem. 2011;11(8):678–94.

Publisher's Note